Characterization of Atherosclerotic Plaques and Mural Thrombi With Intravascular Ultrasound Elastography: A Potential Method Evaluated in an Aortic Rabbit Model and a Human Coronary Artery

Roch Listz Maurice, Jérémie Fromageau, Marie-Hélène Roy Cardinal, Marvin Doyley, Ebo de Muinck, John Robb, and Guy Cloutier, *Senior Member, IEEE*

***Abstract*—Plaque rupture is correlated with the plaque morphology, composition, mechanical properties, and with the blood pressure. Whereas the geometry can accurately be assessed with intravascular ultrasound (IVUS) imaging, intravascular elastography (IVE) is capable of extracting information on the plaque local mechanical properties and composition. This paper reports additional IVE validation data regarding reproducibility and potential to characterize atherosclerotic plaques and mural thrombi. In a first investigation, radio frequency (RF) data were acquired from the abdominal aorta of an atherosclerotic rabbit model. In a second investigation, IVUS RF data were recorded from the left coronary artery of a patient referred for angioplasty. In both cases, Galaxy IVUS scanners (Boston Scientific, Freemont, CA), equipped with 40 MHz Atlantis catheters, were used. Elastograms were computed using two methods, the Lagrangian speckle model estimator (LSME) and the scaling factor estimator (SFE). Corroborated with histology, the LSME and the SFE both clearly detected a soft thrombus attached to the vascular wall. Moreover, shear elastograms, only available with the LSME, confirmed the presence of the thrombus. Additionally, IVE was found reproducible with consistent elastograms between cardiac cycles (CCs). Regarding the human dataset, only the LSME was capable of identifying a plaque that presumably sheltered a lipid core. Whereas such an assumption could not be certified with histology, radial shear and tangential strain LSME elastograms enabled the same conclusion. It is worth emphasizing that this paper reports the first ever *in vivo* tangential strain elastogram with regards to vascular imaging, due to the LSME. It is concluded that the IVE was reproducible exhibiting consistent strain patterns between CCs. The IVE might provide a unique tool to assess coronary wall lesions.**

***Index Terms*—Abdominal aorta, atherosclerosis, coronary arteries, intravascular/endovascular elastography (EVE), intravascular ultrasound (IVUS), Lagrangian speckle model estimator (LSME), rabbit model of atherosclerosis, scaling factor estimator (SFE), vulnerable plaque.**

I. Introduction

INTRAVASCULAR ELASTOGRAPHY (IVE), also known as endovascular elastography (EVE), was introduced to complement intravascular ultrasound (IVUS) echograms in the assessment of vessel wall lesions and for endovascular therapy planning [1]. In IVE, the vascular tissue is usually subjected to the blood flow pulsation, whereas radio frequency (RF) cross-section data are acquired using a catheter-based modality.

A. Correlation-Based Motion Estimators in IVE

The most commonly used motion estimators in IVE applications are 1-D correlation-based techniques. This choice is mainly dictated by the ability of such estimators to be implemented. They may also provide real-time tissue-motion estimates. In such a process, the displacement between pre- and postmotion pairs of RF-lines is determined using cross-correlation analysis. Strain is then computed from the gradient of the displacement field [1], [2]. A different implementation of the 1-D cross-correlation technique was proposed by Brusseau *et al.* [3] to investigate a postmortem human excised carotid artery. They computed an adaptive and iterative estimation of local scaling factors, using the phase information between pre- and postcompression RF signals.

In IVE, the position of the catheter in the lumen is generally neither in the center nor parallel to the vessel axis, and the lumen geometry is generally not circular. According to that, the tissue displacement may be misaligned with the ultrasound beam, introducing substantial decorrelation between tissue pre- and postcompression signals. Regarding that, 1-D estimators may not be optimal if such decorrelation is not appropriately compensated for. Ryan and Foster [4] then proposed a 2-D correlation-based speckle tracking method, which used envelope B-mode data, to compute vascular elastograms. Moreover, the IVE catheter

Manuscript received February 8, 2007. This work was supported by the Natural Sciences and Engineering Research Council of Canada under Grant 312136-06. The work of Dr. Maurice was supported in part by a Research Scholarship Award from the Fonds de la Recherche en Santé du Québec (FRSQ) (2006–2008), and that of Dr. Cloutier by a National Scientist Award of FRSQ (2004–2009).

R. L. Maurice and G. Cloutier are with the Laboratory of Biorheology and Medical Ultrasonics, Research Center, University of Montreal Hospital, Montreal, QC H2L 2W5, Canada. They are also with the Department of Radiology, Radio-Oncology and Nuclear Medicine, and Institute of Biomedical Engineering, University of Montreal, Montreal, QC H3C 3J7, Canada (e-mail: maurice.roch.chum@ssss.gouv.qc.ca; guy.cloutier@umontreal.ca).

J. Fromageau and M.-H. Roy Cardinal are with the Laboratory of Biorheology and Medical Ultrasonics, Research Center, University of Montreal Hospital, Montreal, QC H2L 2W5, Canada (e-mail: j.fromageau@umontreal.ca; roycarmh@IRO.UMontreal.CA).

M. Doyley is with the Thayer School of Engineering, Dartmouth College, Hanover, NH 03755 USA. He is also with the Department of Radiology, Dartmouth Medical School, Hanover, NH 03755 USA (e-mail: doyley@ece.rochester.edu).

E. de Muinck and J. Robb are with the Department of Cardiology, Dartmouth Medical School, Hanover, NH 03755 USA (e-mail: Ebo.D.deMuinck@Dartmouth.EDU; John.F.Robb@Hitchcock.ORG).

Color versions of one or more of the figures in this paper are available online at http://ieeexplore.ieee.org.

Digital Object Identifier 10.1109/TITB.2008.917905

instability due to the blood flow pulsation may constitute an additional source of decorrelation between pre- and postcompression signals. To that, Shapo *et al*. [5], [6] proposed the application of an angioplasty balloon to stabilize the catheter in the vessel lumen along with a 2-D correlation-based *phase sensitive speckle tracking* technique that also used envelope B-mode data. To our knowledge, Ryan and Foster and Shapo et *al*. only presented some *in vitro* vessel-mimicking phantom data, their investigations did not go any further with *ex vivo* or *in vivo* validations.

B. Lagrangian Speckle Model Estimator (LSME)

In addition to the difficulties reported earlier, the heterogeneity of the vascular tissue and of the plaques themselves may induce very complex tissue deformations such as nonrigid rotation, scaling, shear, etc. Whereas most of the current elastographic methods use correlation techniques to assess tissue motion, they may not be optimal to investigate such complex strain patterns. The Lagrangian speckle model estimator (LSME) was then recently proposed for strain computation in EVE [7], [8]. The LSME takes advantage of 2-D correlation analysis for the purpose of *prior* rigid registration, whereas the complete 2-D strain tensor (ε) is further computed as the solution of a nonlinear minimization problem. Albeit the lateral/tangential motion estimates may have large variances due to the low lateral/angular resolution of current IVUS systems, the principal components of ε give information about tissue rigidity and the shear strain parameters might provide insights about plaque vulnerability.

C. Purposes of This Study

The main determinants leading to ruptured plaques are known to be a large lipid core covered by a thin fibrous cap and/or a dense infiltration of macrophages inside the fibrous cap [9]. Using Yucatan pig models of atherosclerosis in iliac and femoral arteries, de Korte *et al*. [10] showed that the IVE was capable of identifying plaque components. Whereas that group [2] previously demonstrated the reproducibility of IVE computed with a correlation-based method in humans, we recently ascertained with the LSME the presence of hard atherosclerotic plaques and soft lipid cores in patients referred for IVUS coronary examinations [11]. The current paper consists of a further validation of IVE assessed with the LSME and the scaling factor estimation (SFE) [12] methods.

In vivo IVE data obtained from the abdominal aorta of an atherosclerotic rabbit model and from the left coronary artery of a patient are reported. Regarding the animal study, the LSME and SFE clearly detected a soft thrombus attached to the vascular wall. Such a finding was corroborated with histology. Moreover, shear elastograms, only available with the LSME, confirmed the presence of the thrombus. Additionally, the IVE was found consistent between cardiac cycles (CCs). Regarding the human investigation, due to the rotation of the IVUS catheter during cardiac contraction, the SFE failed and data are only reported for the LSME. A plaque, which presumably sheltered a lipid core, was identified. Albeit such an assumption could not be certified with histology, radial shear and tangential strain elastograms enabled the same conclusion.

Whereas Lee and Konofagou [13] and our group [14] previously reported lateral strain elastograms from simulated data, it is worth emphasizing that, to our knowledge, this will be the first time that *in vivo* radial strain and shear along with tangential strain elastograms are simultaneously computed with the same datasets and presented. *In vivo* tangential strain elastograms are shown for the first time in the ultrasound literature, whereas our group is the only one that has an algorithm (LSME) that can assess simultaneously all components of the deformation matrix (i.e., radial, tangential strain and shear elastograms). This will also be the first time that consistent elastograms, allowing the dissociation between diastole and systole within the same CC, are published. The discussion emphasizes the potential of IVE to characterize vulnerable atherosclerotic plaques.

II. Methods

A. Animal Model

Abdominal aortic atherosclerosis was induced in a New Zealand white rabbit of 4 kg by employing a combination of balloon angioplasty denudation and a hypercholesterolemic diet (purified rabbit chow supplemented with 0.3% cholesterol and 4.7% coconut oil). The diet lasted two weeks *prior* to angiography denudation and four weeks after denudation. During IVUS data acquisition under X-ray angiography guidance, the position of the tip of the IVUS catheter with respect to the rib cage was identified. The rabbit was then euthanized, the intercostal rib position of the IVUS catheter tip was marked on the abdominal aorta, and a fresh segment of the artery was excised for histology. Sections of the excised vessel were stained with haematoxylin–eosin.

B. Human Subject

The study included one patient with unstable angina pectoris who was referred for percutaneous coronary intervention. After intravenous administration of 10 000 IU of heparin and 200 mg of acetylsalicylic acid, a 6 French guiding catheter was advanced up to the ostium of the left coronary artery. After injection of a bolus of 3 mg of isosorbide dinitrate, a preintervention IVUS assessment was performed. The patient signed a written informed consent *prior* to the examination.

C. Experimental Setup

The equipment used for elastographic imaging consisted of a Galaxy IVUS scanner (Boston Scientific/Scimed, Freemont, CA) that was equipped with 40 MHz Atlantis Pro, single-element rotating catheters, and a modified DP310 12 bits 400 MS/s PCI-bus data acquisition card (Acqiris, Geneva, Switzerland). The image acquisition frame rate was 30 Hz. The time-sequence dataset recorded from the rabbit's abdominal aorta, at a fixed axial position of the catheter (i.e., without pullback), contained 126 cross-sectional images of 2048 samples $\times$ 256 RF lines. Whereas the raw RF data were used to compute elastograms, Fig. 1(a) presents one such RF image that was postprocessed with envelop detection and logarithmic compression for illustration purpose. For both the SFE and LSME, eight CCs were investigated; that provided 88 elastograms computed

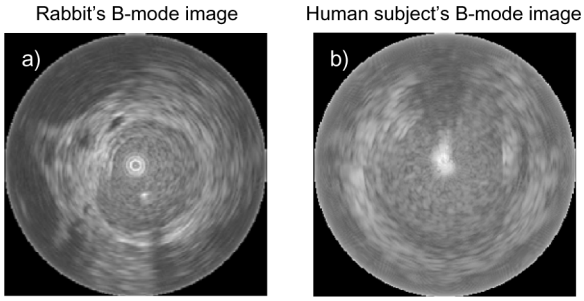

Fig. 1. (a) Cross-sectional B-mode image acquired from the rabbit's abdominal aorta. (b) Cross-sectional B-mode image acquired from the human subject's left coronary artery.

between each pair of consecutive RF images, respectively. To avoid redundancy, elastograms are displayed for two CCs, arbitrarily the first and the last CC in the sequence.

For the human's coronary artery, the time-sequence dataset contained seven cross-sectional images of 2048 samples $\times$ 256 RF lines also acquired at a fixed axial position of the catheter. Similarly, Fig. 1(b) presents a RF image that was postprocessed with envelop detection and logarithmic compression. On the other hand, coronary arteries are subjected to relatively strong rotation movement that follows the heart motion, inducing very substantial decorrelation within the time-sequence RF data. Because of that, 1-D SFE failed to compute reliable elastograms. Results are then reported only for the LSME.

D. Lagrangian Speckle Model Estimator (LSME)

The LSME is described in details elsewhere [7]. It is worth emphasizing that the first step of the LSME consists in a rigid registration that allows compensating for potential translation movement using 2-D cross-correlation analysis. From such a process, radial/axial and circumferential/lateral displacement fields and correlation coefficient distributions are computed. As it will be presented later, the radial displacement field was used in this study to distinguish between the systolic and diastolic phases of the CC because no electrocardiogram (ECG) gated acquisitions were available, whereas the correlation coefficient distribution was used to initiate the semiautomatic segmentation procedure of the vessel wall. Contrarily to conventional correlation-based estimators that use the gradient of the radial displacement to compute the radial strain elastogram, the LSME was formulated as a nonlinear minimization problem that allows assessing the complete 2-D deformation matrix (Δ). It is worth remembering that, in the context of IVE, Δ can mathematically be defined as [7]

$$\Delta = \begin{bmatrix} \dfrac{\partial U_\varphi}{\partial \varphi} & \dfrac{\partial U_\varphi}{\partial r} \\ \dfrac{\partial U_r}{\partial \varphi} & \dfrac{\partial U_r}{\partial r} \end{bmatrix}. \tag{1}$$

In this equation, U_r and U_φ are the radial and tangential displacement fields, respectively. The four components of Δ, in this specific polar coordinates' formulation, are Δ_{rr}, $\Delta_{r\varphi}$, $\Delta_{\varphi\varphi}$, and $\Delta_{\varphi r}$, being the radial strain and shear, and tangential strain and shear, respectively. The map of the distribution of each component of Δ (Δ_{ij}) provides a specific elastogram. It is also worth mentioning that Δ relates the strain tensor ε through the following equation:

$$\varepsilon_{ij}(t) = \frac{1}{2}[\Delta_{ij}(t) + \Delta_{ji}(t)]. \tag{2}$$

As presented in details elsewhere [15], the LSME numerical solution was reached using an inversion algorithm. Local deformation parameters (Δ_{ij}) were computed using small 2-D measurement windows (MWs) on RF images (385 $\times$ 310 μm^2), with 90% axial and lateral overlaps. With the purpose of improving elastograms' SNR, the LSME elastograms were low-pass filtered using a 1 $\times$ 1 pixel (130 $\times$ 130 μm^2) kernel Gaussian filter. Note that the pixel size in square micrometers differed between RF images and elastograms (it is larger for elastograms).

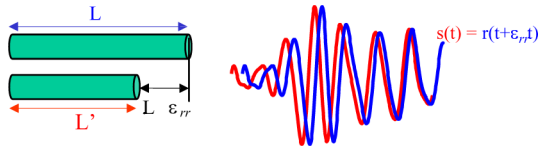

Fig. 2 (color on-line). Modeling of the deformed 1-D signal $s(t)$, from the reference signal $r(t)$, with the assumption that a deformation can be considered as a scaling factor.

E. Scaling Factor Estimator (SFE)

As illustrated in Fig. 2, the SFE is a 1-D estimator that is based on the classical linear elasticity theory. In this case, the radial strain, Δ_{rr} ($= \varepsilon_{rr}$) in (1) and (2), is assessed using a correlation-based method [12], maximizing the function

$$R_{rs}(\hat{\varepsilon}_{rr}) = \int_0^T r(t) \times s(t - \hat{\varepsilon}_{rr} t)\, \mathrm{d}t \tag{3}$$

with $\hat{\varepsilon}_{rr}$ being the estimation of ε_{rr}. Unlike the LSME, the SFE performed the numerical solution for small 1-D window length ($T = 317$ μm) over given regions of interest to provide local estimations of Δ_{rr}. No rigid registration was used prior to computing (3). Similarly to the LSME, SFE elastograms were low-pass filtered using a 1 $\times$ 1 pixel (130 $\times$ 130 μm^2) kernel Gaussian filter.

F. Segmentation Procedure

For the purpose of the present study, a semiautomatic segmentation of the vessel wall was used. Developed by our group [16], the segmentation model is based on the fast-marching method and uses gray level gradients and gray level probability density functions of the vessel wall structures and blood. The contours of the wall were manually initiated on the first image of each sequence, said $I(x(t_0), y(t_0))$, based on the correlation coefficient map between $I(x(t_0), y(t_0))$ and $I(x(t_1), y(t_1))$. The contours that resulted from the segmentation process of a given $I(x(t), y(t))$ were then used to initiate the segmentation of $I(x(t+\Delta t), y(t+\Delta t))$. Fig. 3 illustrates the different steps of the segmentation procedure, starting with Fig. 3(a) that displays a polar B-mode IVUS image. Fig. 3(b) presents the correlation

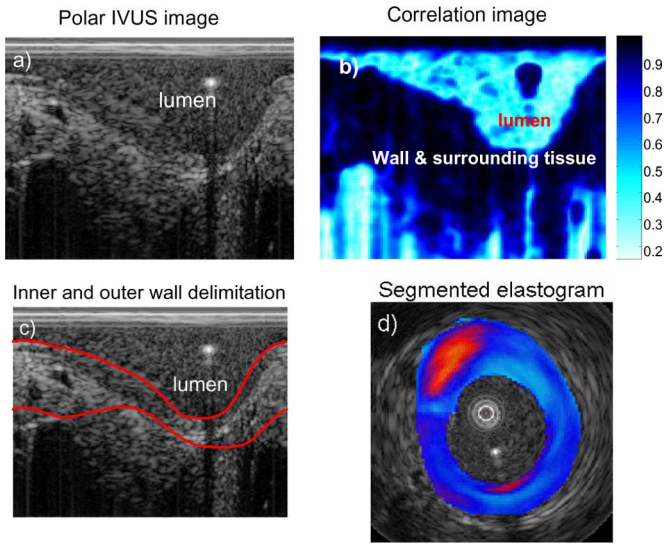

Fig. 3 (color on-line). Illustration of the vessel wall segmentation. (a) Polar B-mode IVUS image. (b) Correlation coefficient map that was used to initiate the segmentation procedure. (c) Segmentation of the inner and outer walls using a semiautomatic procedure that is based on the fast-marching method, and on gray level gradients and gray level probability density functions of the vessel wall structures and blood. (d) Resulting segmented radial strain elastogram superimposed on the Cartesian IVUS image.

coefficient map that was used to initiate the segmentation procedure, whereas Fig. 3(c) presents the IVUS image along with the wall contours computed with the segmentation process. Fig. 3(d) exhibits a segmented radial strain elastogram, in Cartesian coordinates, that superimposes the IVUS image.

G. Cardiac Cycle Curve (CCC)

The ECG having not been available along with the RF data for analysis, we used the following alternative. Because it consisted of a curve that allows following the CC phases (systole/diastole), we labeled it as the *cardiac cycle curve* (CCC). To summarize, the wall radial displacement field, which was computed along with the LSME, was used to identify the CC phases. In such a context, positive and negative displacements for a selected *plaque-free* region of interest within the wall were associated with systole and diastole, respectively. Note that this preprocessing was only performed for the rabbit dataset because the number of RF images available for the human coronary vessel did not cover a whole CC. Fig. 4 illustrates the procedure with the thick blue line being the displacement curve, while the thin red line gives the CCC. The CCC is presented as a squared wave only for the purpose of clarity and simplification. An average of 12 ± 0.82 RF images per CC was found. To avoid redundancies, elastograms are displayed only for the first and last CC of the sequence to illustrate the reproducibility of IVE.

III. Results

It is worth emphasizing that the RF data were acquired by the coauthors from Dartmouth Medical School and were analyzed blindly by the Montreal group; consequently, no information was provided about the acquisition procedures and about pathologies to be observed.

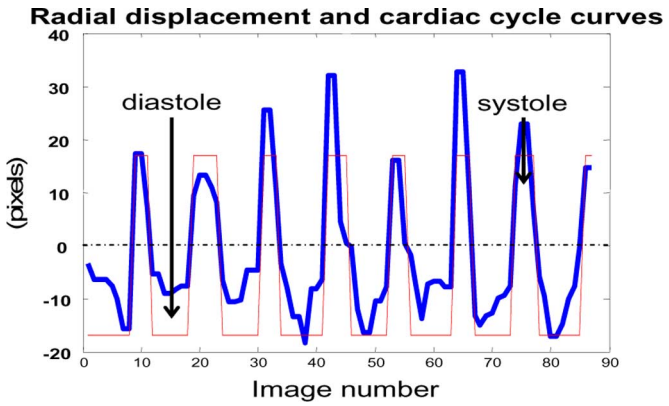

Fig. 4 (color on-line). Illustration of the CCC. The thick blue line gives the effective radial displacement curve as a function of image number (equivalently as a function of time) for a selected *plaque-free* region of interest within the wall. The thin red line gives the CCC, presented as a squared wave for the purpose of clarity. In this context, positive and negative displacements are associated with systole and diastole, respectively.

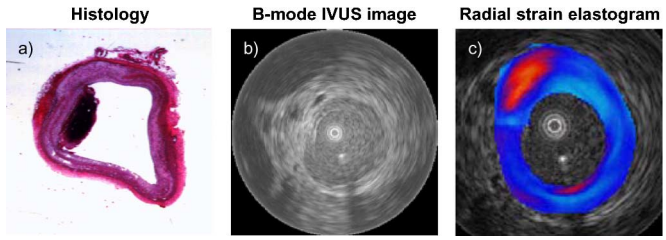

Fig. 5 (color on-line). (a) Histology picture obtained from the excised rabbit's abdominal aorta. A haematoxylin–eosin staining was used. (b) Cross-sectional B-mode IVUS image. (c) LSME radial strain elastogram, superimposed on the IVUS image.

A. Animal Study

Fig. 5(a) displays a histology picture obtained from the excised abdominal aorta. A thrombus that is attached to the vessel wall is observed between 9 o'clock and 12 o'clock. Interestingly, the thrombus was not clearly identified with B-mode IVUS as illustrated in Fig. 5(b). On the other hand, Fig. 5(c) maps a LSME radial strain elastogram, superimposed on the IVUS image, which clearly allows detecting the mural thrombus.

1) Reproducibility and Qualitative Comparisons Between LSME and SFE: Fig. 6 maps the CCC along with the radial strain elastograms that were computed for two CCs with the LSME. These elastograms were superimposed on the reconstituted B-mode IVUS images only for the purpose of illustration. In this configuration, positive strain values displayed in blue are associated with tissue dilation, whereas negative strains displayed in red and yellow are indicative of tissue compression. From Fig. 6(a)–(h), the elastograms correspond to the diastolic phase (reduction of the lumen diameter, dilatation of the healthy vascular wall presented with a blue colormap and compression of the mural thrombus, displayed between 9 o'clock and 12 o'clock, with a red map), whereas Fig. 6(i) and (j) consist of the systolic phase (increase in lumen diameter, compression of the vascular wall and dilatation of the thrombus). Similarly, elastograms from Fig. 6(k)–(t) map another CC to illustrate the reproducibility of IVE between

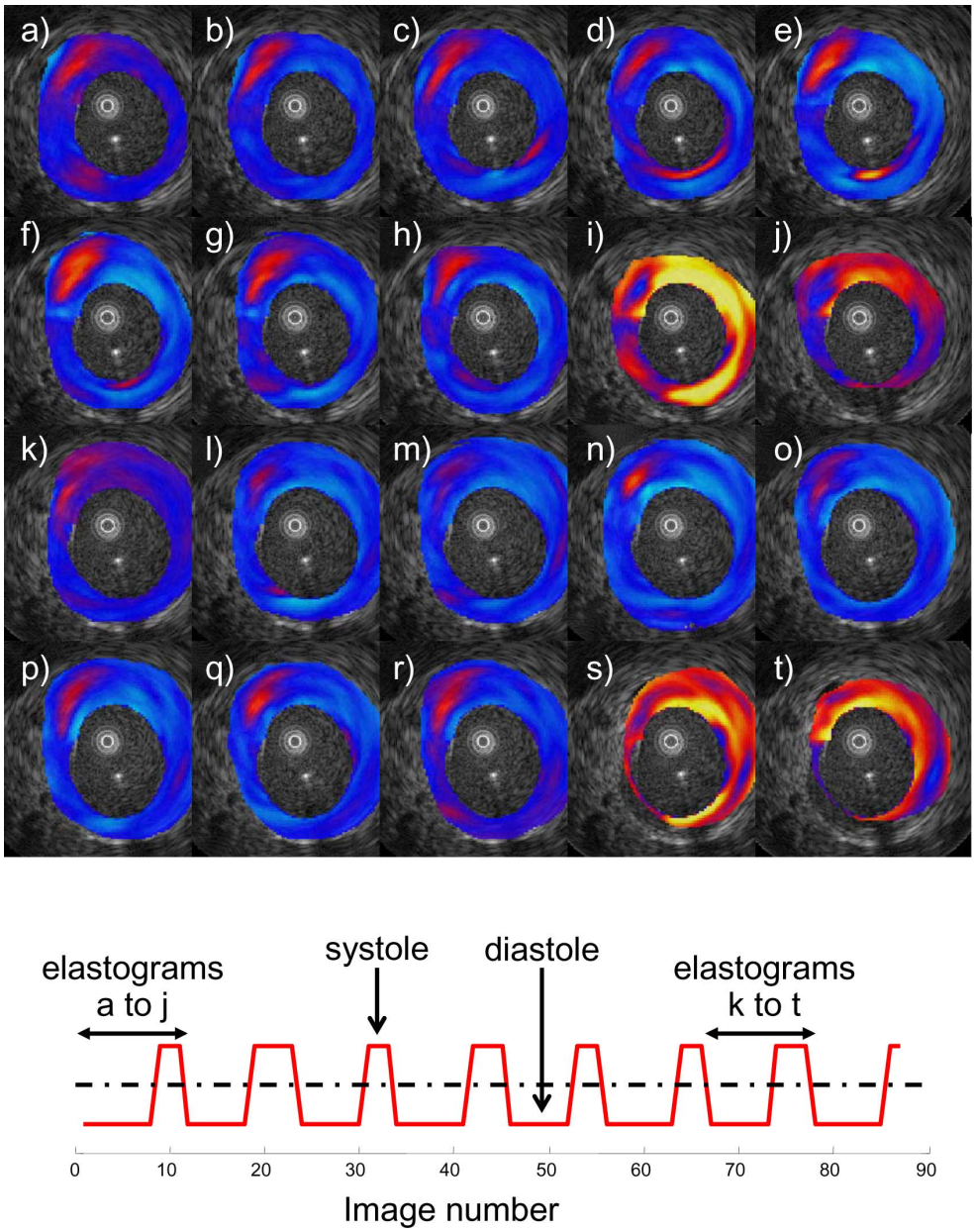

Fig. 6 (color on-line). (a)–(t) Radial strain elastograms computed for two CCs over the rabbit's abdominal aorta with the LSME. In this configuration, positive strain values displayed in blue are associated with tissue dilation, whereas negative strains displayed in red and yellow are indicative of tissue compression. For the purpose of illustration, the colormap was normalized in a range of $[-2.5$ to $2]\%$. The CCC, plotted at the bottom of this figure, traces the different moments (systole/diastole) of the CC.

CCs. It is to note that the systolic elastograms presented in Fig. 6(i), (j), (s), and (t) are noisier due to the larger movements of the vessel wall at that moment of the CC and possible IVUS catheter displacement with the flow. While not presented here, these patterns were observed to be repetitive over all cycles available, indicating the reproducibility of the method.

Equivalently, Fig. 7 presents elastograms that were computed with the SFE for the same two CCs as the LSME. These results are in accordance with those obtained with the LSME, indicating the presence of a mural thrombus between 9 o'clock and 12 o'clock. However, SFE elastograms look noisier.

2) Thrombus Characterization: As observed in Figs. 6 and 7, the mural thrombus apparently changed in size and geometry from diastole to systole. Nevertheless, the thrombus detectability appears optimal mostly in the second half of diastole where the vessel wall is more stable. In addition, one can observe inverse strain values between the thrombus and the surrounding vascular tissue. An explanation for the opposite direction of the strain for both tissue structures is given in Section IV.

Complementarily to the radial strain elastograms (Δ_{rr}) of Figs. 6 and 7, we now present in Fig. 8 radial shear elastograms ($\Delta_{r\varphi}$) that were computed with the LSME during the diastolic phase. These shear elastograms are characterized by

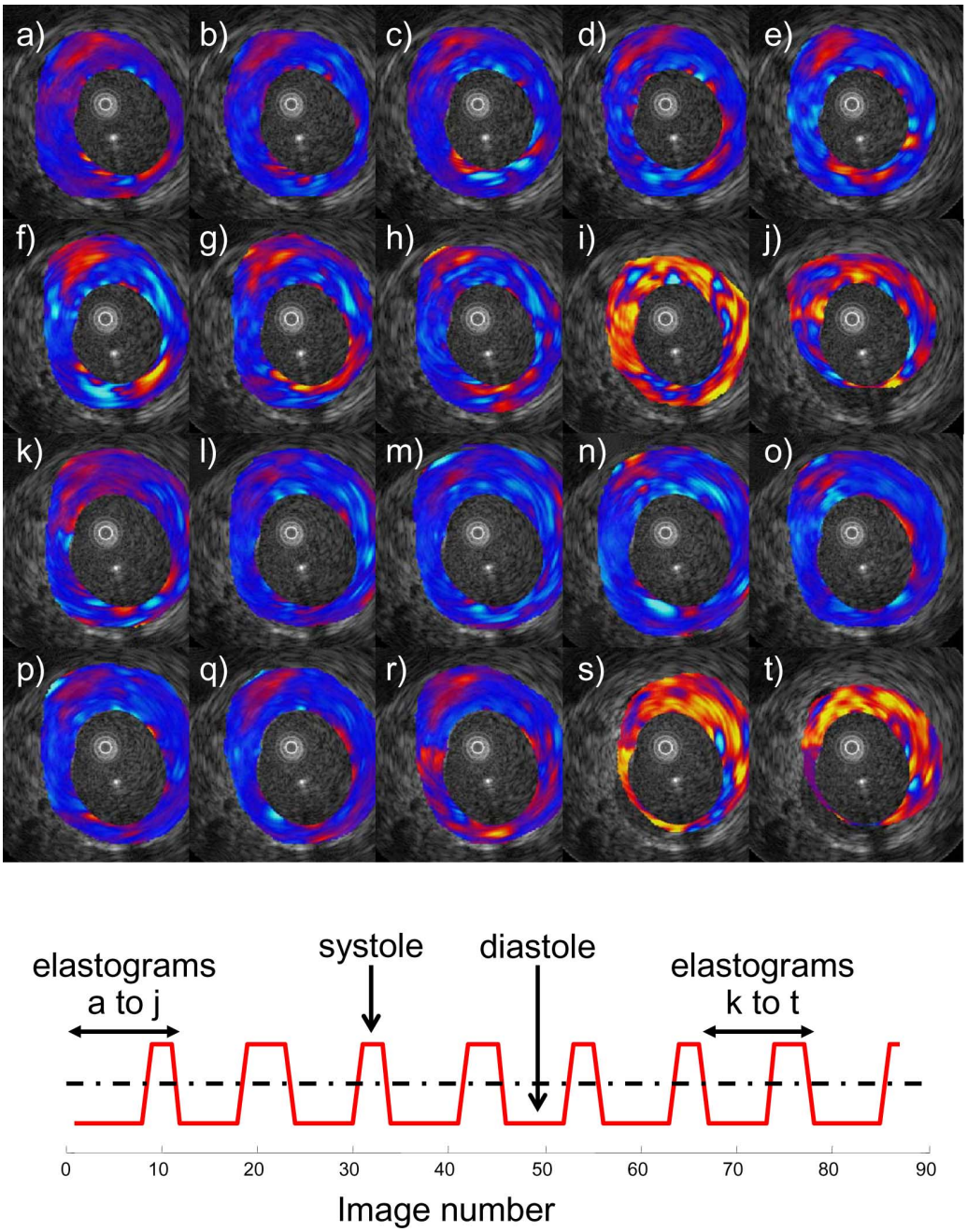

Fig. 7 (color on-line). (a)–(t) Radial strain elastograms computed for two CCs over the rabbit's abdominal aorta with the SFE. In this configuration, positive strain values displayed in blue are associated with tissue dilation, whereas negative strains displayed in red and yellow are indicative of tissue compression. For the purpose of illustration, the colormap was normalized in a range of $[-3.5 \text{ to } 3]\,\%$. The CCC, plotted at the bottom of this figure, traces the different moments (systole/diastole) of the CC.

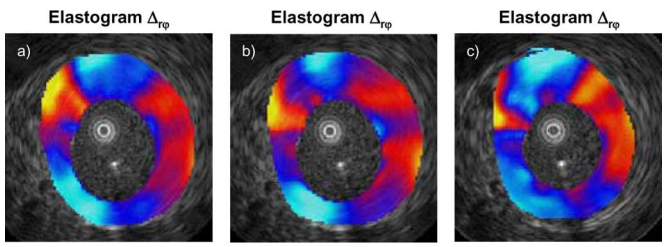

Fig. 8 (color on-line). Radial shear elastograms ($\Delta_{r\varphi}$) computed with the LSME. For the purpose of illustration, the colormap was normalized in a range of $[-2.5 \text{ to } 2]\,\%$.

cohabitation of high positive and negative shear values within the mural thrombus. This tends to corroborate the hypothesis of soft materials in that area surrounded by more rigid vessel components promoting such inhomogeneities of the mechanical properties and concentration of shear.

B. Human Study

As for the rabbit's data, the four components of Δ were computed for each pair of consecutive RF images, providing six estimations of Δ labeled as Δ_{ij} for different t_n (n $\in [1, 6]$). Fig. 9(a) and (b) shows two radial strain elastograms (Δ_{rr}) at

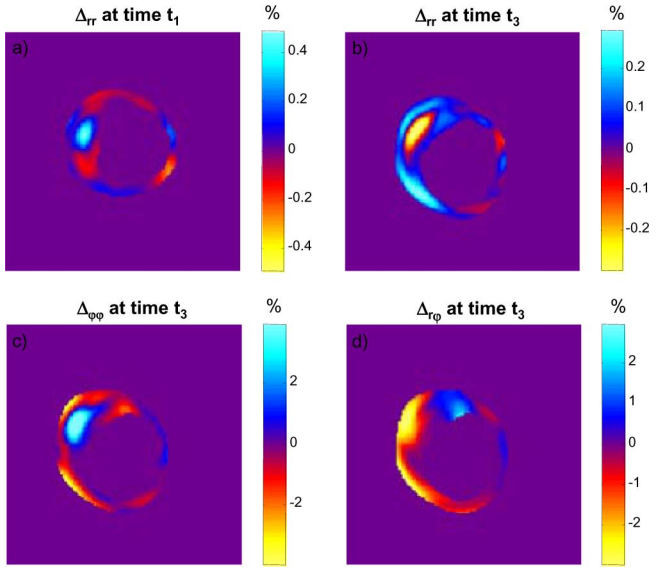

Fig. 9 (color on-line). (a) Radial strain elastogram (Δ_{rr}) computed in end diastole over the left coronary artery of a patient with an atherosclerotic plaque. (b) Radial strain elastogram (Δ_{rr}) computed in early systole. (c) Tangential strain elastogram ($\Delta_{\varphi\varphi}$) computed in early systole. (d) Radial shear elastogram ($\Delta_{r\varphi}$) also computed in early systole. The colorbar gives the strain in percent.

times t_1 and t_3 (in end diastole for t_1 and early systole for t_3; note that flow and lumen vessel extension occur in diastole for coronary arteries). The colorbar gives the strain in percent. Here again, the blue mapping (positive strain values) is associated with radial tissue dilatation (equivalent to tangential shrinking), whereas red/yellow colors (negative strain values) are related to radial tissue compression (equivalent to tangential extension).

Fig. 9(a) shows that the "normal" vessel wall between 10 o'clock and 7 o'clock is on average under compression in diastole. A plaque area, around 9 o'clock, exhibits the opposite characteristics, suggesting the presence of a soft material. Some "mechanical artifacts" [14] are, however, observed. Fig. 9(b) presents the reverse mechanical behavior in systole (emptying of the vessel). A slight rotation of the IVUS catheter most likely occurred between t_1 and t_3 since the soft plaque is now observed around 10 o'clock.

Fig. 9(c) presents a tangential strain elastogram ($\Delta_{\varphi\varphi}$) at time t_3. As expected, due to the incompressibility of biological soft tissues, the $\Delta_{\varphi\varphi}$ elastogram exhibits opposite mechanical characteristics with respect to the equivalent Δ_{rr} elastogram. In other words, an expansive radial behavior of the vessel wall corresponds to a compressive tangential behavior, and inversely for the plaque. Fig. 9(d) maps the radial shear elastogram ($\Delta_{r\varphi}$) at time t_3. As for the rabbit data, this shear elastogram is characterized by cohabitation of high positive and negative shear values in the plaque area. This likely supports the hypothesis that the plaque embedded a soft material (lipid pool).

IV. Discussion

A. About the Rabbit Study

This paper reported IVE data obtained from a rabbit's model of atherosclerosis. The abdominal aorta was scanned and two methods were used to compute the elastograms, namely the SFE and the LSME. The radial strain and shear elastograms were corroborated by histology where a mural thrombus was identified.

With both methods, the thrombus was found to deform inversely (positive/negative) with respect to the normal wall region. Additionally, high shear values were detected within the mural thrombus, which likely is indicative of neighboring materials (soft thrombus and more rigid wall) having different rigidities. These results suggest that the fresh soft thrombus rigidly attached to the wall expanded radially in systole due to the blood pressure increase that likely compressed (squeezed) its side, and inversely in diastole. Although supported by the displayed elastograms, modeling of mural thrombi with different geometries and under different hemodynamic conditions would be required to fully state on the validity of this hypothesis. Furthermore, the IVE was found reproducible with consistent elastograms within each CC. The IVE was also found reproducible between several CCs. However, because of the largest vessel wall movement during systole, target detectability (the thrombus in this case) appears optimal in the second half of diastole.

Through observation of Figs. 6 and 7, the LSME outperformed the SFE with more uniform elastograms along with a better target detectability. The main reason behind this stems from the fact that the SFE is a 1-D estimator in a 1-D direction whereas the LSME is a 2-D model-based estimator. Because the vessel wall was subjected to complex movements such as rotations, shears, compression/dilation, etc., the 1-D SFE was more sensitive to signal decorrelation. Additionally, the LSME uses rigid registration prior to motion estimation to compensate for artefactual movements (such as catheter rotation, for example) whereas the SFE does not. This becomes more obvious in the case of the human subject, where the SFE was not capable of computing consistent elastograms (results not shown). In this context, the proximity of the heart indeed induces instability to the vessel wall or/and to the catheter, and then, decorrelation is amplified between pre- and postmotion signals, thus restricting 1-D SFE performances. On the other hand, the SFE presents the advantage of a faster computation time.

Furthermore, the contrast-to-noise ratio (CNR),[1] which was defined by Bilgen [17] as a measure of target detectability in elastography, was used for a quantitative comparison between the LSME and the SFE with regards to thrombus detection for the rabbit's data during diastole. LSME-CNR was found higher than SFE-CNR by a factor of 3 (91/30), indicating a better LSME thrombus detectability. In addition, it is to note that target detectability is also dependent on the MW. In general, targets that are smaller than half the MW may be missed by elastography.

B. About the Human Subject Study

This paper also reported IVE data obtained from an atherosclerotic left coronary artery of a human subject. Only

[1]The CNR is formulated as $(s_t - s_b)^2/[(\mathrm{var}(\hat{s}_t/s_t) + \mathrm{var}(\hat{s}_t/s_t))/2]$ with s_t and s_b being the target and background strains, respectively.

LSME data were reported, the SFE was not able to compute consistent elastograms. A region made of material softer than the arterial wall was detected between 9 o'clock and 12 o'clock. Whereas this cannot be confirmed, our results tend to suggest that a lipid core was present in the plaque area. Due to the complex kinematics of plaque structures, either postmortem histology or modeling would allow to confirm this hypothesis. On the other hand, the "normal" vessel wall was sometimes misidentified due to its minute thickness. This, at least, partly justifies the mechanical (brightening and darkening) artifacts located between 6 o'clock and 9 o'clock.

We expected to observe large variances in the tangential strain estimate of Fig. 9(c) because of the limited tangential (circumferential) resolution of IVUS systems. Due to the robustness of the LSME, it was possible to compute at least one very representative tangential elastogram ($\Delta_{\varphi\varphi}$) with our dataset. This also may partially be attributed to the good RF data quality and high SNR. To our knowledge, this is the first *in vivo* tangential strain elastogram (equivalent to lateral strain in Cartesian coordinates) to be reported in the literature of vascular elastography. It is worth emphasizing that the radial and tangential strain and radial shear elastograms exhibited a very consistent and convincing perspective. This could be seen as a major finding regarding the *elastographic* community, and we believe that the quality of our elastograms (especially those computed with the LSME) could be of clinical value. On the other hand, the tangential elastogram shows higher strain values in comparison to the radial elastograms of Fig. 9(a) and (b). Although not investigated yet, this may be related to the anisotropic nature of the vascular tissue or/and to the algorithm implementation.

C. About Shear Elastograms and Plaque Vulnerability

A major advantage of the LSME is that it computes the complete 2-D deformation matrix. Whereas the radial strain dictates the rigidity of the vascular materials (soft and hard), the shear may give insights about plaque vulnerability by indicating plaque prone to rupture in regions subjected to high stresses. Indeed, the occurrence of shear stress within the normal arterial wall of arteries was recently demonstrated [18]. It was hypothesized that the long-term effect of this stress could weaken a material and increase its risk of rupture. Similarly, it could be hypothesized that high shear deformation would promote plaque hemorrhage, inflammation, and increase its risk to rupture. Because of the complex composition and kinematics of atherosclerotic plaques, we are aware that further validations are required to fully conclude on the quantitative potential of IVE. However, the results reported here indicate that IVE could become a clinical marker of plaque vulnerability.

V. Conclusion

This paper reported elastographic data for a rabbit model of atherosclerosis and for a pathologic left coronary artery of a human subject. Regarding the rabbit's data, radial elastograms computed with two different methods allowed detecting the soft mural thrombus that was identified by histology. Furthermore, this observation was supported by shear elastograms, due to the LSME. This latter parameter might have a major relevance, since it may provide insights about plaque vulnerability. Regarding the human subject's data, radial and tangential strain and radial shear elastograms were computed with the LSME. In summary, the clinical relevance of IVE is, at least, twofold. Whereas radial, and eventually tangential strain elastograms might allow distinguishing plaque components, radial shear elastograms might give insights about plaque vulnerability.

Acknowledgment

The authors acknowledge Dr. T.-J. Tao, Senior Research Fellow, Boston Scientific Corporation, Imaging Division, for providing the RF IVUS data used in this study.

References

[1] C. L. de Korte, E. I. Céspedes, A. F. W. van der Steen, and C. T. Lancée, "Intravascular elasticity imaging using ultrasound—Feasibility studies in phantoms," *Ultrasound Med. Biol.*, vol. 23, no. 5, pp. 735–746, 1997.

[2] C. L. de Korte, A. F. W. van der Steen, E. I. Céspedes, G. Pasterkamp, S. G. Carlier, F. Mastik, A. H. Schoneveld, P. W. Serruys, and N. Bom, "Characterization of plaque components and vulnerability with intravascular ultrasound elastography," *Phys. Med. Biol.*, vol. 45, no. 6, pp. 1465–1475, 2000.

[3] E. Brusseau, J. Fromageau, G. Finet, P. Delachartre, and D. Vray, "Axial strain imaging of intravascular data: Results on polyvinyl alcohol cryogel phantoms and carotid artery," *Ultrasound Med. Biol.*, vol. 27, no. 12, pp. 1631–1642, 2001.

[4] L. K. Ryan and F. S. Foster, "Ultrasonic measurement of differential displacement strain in a vascular model," *Ultrason. Imag.*, vol. 19, no. 1, pp. 19–38, 1997.

[5] B. M. Shapo, J. R. Crowe, A. R. Skovoroda, M. J. Eberle, N. A. Cohn, and M. O'Donnell, "Displacement and strain imaging of coronary arteries with intraluminal ultrasound," *IEEE Trans. Ultrason., Ferroelectr., Freq. Control*, vol. 43, no. 2, pp. 234–246, Mar. 1996.

[6] B. M. Shapo, J. R. Crowe, R. Erkamp, S. Y. Emelianov, M. J. Eberle, and M. O'Donnell, "Strain imaging of coronary arteries with intraluminal ultrasound: Experiments on an inhomogeneous phantom," *Ultrason. Imag.*, vol. 18, no. 3, pp. 173–191, 1996.

[7] R. L. Maurice, J. Ohayon, G. Finet, and G. Cloutier, "Adapting the Lagrangian speckle model estimator for endovascular elastography: Theory and validation with simulated radio-frequency data," *J. Acoustical Soc. Amer.*, vol. 116, no. 2, pp. 1276–1286, 2004.

[8] R. L. Maurice, É. Brusseau, G. Finet, and G. Cloutier, "On the potential of the Lagrangian speckle model estimator to characterize atherosclerotic plaques in endovascular elastography: In vitro experiments using an excised human carotid artery," *Ultrasound Med. Biol.*, vol. 31, pp. 85–91, 2005.

[9] V. Fuster, P. R. Moreno, Z. A. Fayad, R. Corti, and J. J. Badimon, "Atherothrombosis and high-risk plaque. Part I: Evolving concepts," *J. Amer. College Cardiol.*, vol. 46, pp. 937–954, 2005.

[10] C. L. de Korte, M. J. Sierevogel, F. Mastik, C. Strijder, J. A. Schaar, E. Velema, G. Pasterkamp, P. W. Serruys, and A. F. W. van der Steen, "Identification of atherosclerotic plaque components with intravascular ultrasound elastography in vivo: A Yucatan pig study," *Circulation*, vol. 105, pp. 1627–1630, 2002.

[11] R. L. Maurice, J. Fromageau, É. Brusseau, G. Finet, and G. Cloutier, "On the potential of the Lagrangian speckle model estimator for endovascular elastography: In vivo human coronary study," *Ultrasound Med. Biol.*, vol. 33, no. 8, pp. 1199–1205, 2007.

[12] J. Fromageau, J.-L. Gennisson, C. Schmitt, R. L. Maurice, R. Mongrain, and G. Cloutier, "Estimation of polyvinyl alcohol cryogel mechanical properties with four ultrasound elastography methods and comparison with gold standard testings," *IEEE Trans. Ultrason., Ferroelectr., Freq. Control*, vol. 54, no. 3, pp. 498–509, Mar. 2007.

[13] W.-N. Lee and E. E. Konofagou, "Analysis of 3D motion effects in myocardial elastography," in *Proc. IEEE Ultrason. Symp.*, Oct. 2006, pp. 1217–1220.

[14] R. L. Maurice, J. Ohayon, Y. Frétigny, M. Bertrand, G. Soulez, and G. Cloutier, "Non-invasive vascular elastography: Theoretical framework," *IEEE Trans. Med. Imag.*, vol. 23, no. 2, pp. 164–180, Feb. 2004.

[15] R. L. Maurice, M. Daronat, J. Ohayon, É. Stoyanova, S. F. Foster, and G. Cloutier, "Non-invasive high-frequency vascular ultrasound elastography," *Phys. Med. Biol.*, vol. 50, pp. 1611–1628, 2005.
[16] M.-H. Roy Cardinal, J. Meunier, G. Soulez, R. L. Maurice, E. Therasse, and G. Cloutier, "Intravascular ultrasound image segmentation: A three-dimensional fast-marching method based on gray level distributions," *IEEE Trans. Med. Imag.*, vol. 25, no. 5, pp. 590–601, May 2006.
[17] M. Bilgen, "Target detectability in acoustic elastography," *IEEE Trans. Ultrason., Ferroelectr., Freq. Control*, vol. 46, no. 5, pp. 1128–1133, Sep. 1999.
[18] J. M. U.-King-Im, Z. Y. Li, R. A. Trivedi, S. Howarth, M. J. Graves, P. J. Kirkpatrick, and J. H. Gillard, "Correlation of shear stress with carotid plaque rupture using MRI and finite element analysis," *J. Neurol.*, vol. 253, no. 3, pp. 379–381, 2006.

Roch L. Maurice received the Ph.D. degree in biomedical engineering from the University of Montreal, Montreal, QC, Canada, in 1998.

He is currently a Scientist at the University of Montreal Hospital Research Center, a Research Assistant Professor in the Department of Radiology, Radio-Oncology and Nuclear Medicine at the University of Montreal, where he is also a member of the Institute of Biomedical Engineering. His current research interests include mathematical modeling for the purpose of characterizing soft biological tissues with specific applications in cardiovascular and breast cancer fields using ultrasound.

Jérémie Fromageau received the M.S. degree in physical acoustics from the University Denis Diderot, Paris, France, in 1999, and the Ph.D. degree in medical image processing from the Institut National des Sciences Appliquées (INSA), Lyon, France, in 2003.

He is currently a Research Associate in the Laboratory of Biorheology and Medical Ultrasonics, University of Montreal Hospital Research Center, Montreal, QC, Canada. His current research interests include signal and image processing applied to medical ultrasound imaging, elastography, and high-frequency imaging.

Marie-Hélène Roy Cardinal obtained the B.Eng. degree in computer engineering from the École Polytechnique de Montréal, Montréal, QC, Canada, in 2001. She is currently working toward the Ph.D. degree in the Laboratory of Biorheology and Medical Ultrasonics, University of Montreal Hospital Research Center, Montreal, QC, Canada.

Her current research interests include medical ultrasound image processing and segmentation.

Marvin M. Doyley received the B.Sc. degree in applied physics from Brunel University, London, U.K., in 1994, and the Ph.D. degree in biophysics from the University of London, London, in 1999.

From 1999 to 2001, he was engaged in research on intravascular ultrasonic elastography in the Department of Experimental Echocardiography of the Thoraxcenter, Erasmus University of Rotterdam, The Netherlands. In 2001, he joined the Department of Radiology, Dartmouth-Hitchcock Medical Center, Hanover, NH. He also joined the Thayer School of Engineering, Dartmouth College, Hanover, in 2001, and is currently an Assistant Professor of engineering. His current research interests include numerical modeling, ultrasonic and magnetic resonance imaging, tissue characterization, image processing, and inverse problem solution.

Ebo de Muinck received the MD and Ph.D. degrees in medicine and cardiology from the University of Groningen, The Netherlands, in 1983 and 1994, respectively.

In 2002, he joined the Section of Cardiology at Dartmouth Medical School, Hanover, NH, where he served as a Director of Pre-clinical Research at the Angiogenesis Research Center. He is currently an Associate Professor of medicine and physiology at the Dartmouth Medical School. His current research interests include developing novel imaging approaches for visualizing plaque angiogenesis.

Dr. de Muinck has served on several peer-review committees for the National Institutes of Health. He is also the recipient of several awards including the Pfizer/ACCF Visiting Professorship award in Cardiovascular medicine, and awards from the National Institutes of Health, Philips Électronics North America, and the Netherlands Heart Foundation.

John F. Robb received the B.A. degree in biology and psychology from Wesleyan University, Middletown, CT, and the M.D. degree (with honors) from Indiana University, Bloomington, in 1979.

He attended the Graduate School in Anatomy and Physiology at Indiana University. He completed Internal Medicine residency and Cardiology fellowship at the University of Minnesota Hospitals and Clinics. In 1985, he joined the Section of Cardiology, Dartmouth-Hitchcock Medical Center, Hanover, NH, where he is currently the Director of the Interventional Cardiology and also an Associate Professor of medicine at the Dartmouth Medical School. From 1998 through 2006, he has been the Medical Director of the Cardiac Care Unit, the Director of the Interventional Cardiology Fellowship Program, the Medical Director of the Angioplasty Special Care Unit, and the Director of the Cardiac Catheterization Laboratories. He is Board Certified in Internal Medicine, Cardiology, and Interventional Cardiology.

Guy Cloutier (S'89–M'90–SM'07) received the B.Eng. degree in electrical engineering from the Université du Québec à Trois-Rivières, Trois-Rivières, QC, Canada, in 1983, and the M.Sc. and Ph.D. degrees in biomedical engineering from the Ecole Polytechnique de Montréal, Montréal, QC, in 1986 and 1990, respectively.

Between 1990 and 1992, he was a Postdoctoral Fellow at the Laboratory of Medical Ultrasonics, Bioengineering Program, The Pennsylvania State University, University Park, PA. He is currently the Director of the Laboratory of Biorheology and Medical Ultrasonics, Research Center of the University of Montreal Hospital, Montreal, QC. He is a Member of the Institute of Biomedical Engineering, University of Montreal, Montreal, where he is also a Professor in the Department of Radiology, Radio-Oncology and Nuclear Medicine. His current research interests include the characterization of red blood cell aggregation dynamics with ultrasound and rheological methods, the development of small animal imaging methods to study blood flow disorders, the characterization of biomechanical properties of vascular wall structures with ultrasound elastography, the 3-D morphologic and hemodynamic assessment of lower limb arterial stenoses, and mathematical and biomechanical modeling. He is the author or coauthor of more than 90 published peer-reviewed papers and book chapters in these fields. He holds six patents (pending). He is a member of the Advisory Editorial Board for the journals *Ultrasound in Medicine and Biology*, *Current Medical Imaging Reviews*, and *Medical Physics* (Guest Associate Editor).

Prof. Cloutier has served on several grant review study sections of the Heart and Stroke Foundation of Canada, the Canadian Institutes of Health Research, the Fonds de la Recherche en Santé du Québec (FRSQ), the Canada Research Chairs, and the National Institutes of Health of the United States. He is the recipient of the National Scientist Award from FRSQ, 2004–2009.